

Supporting Information

Anisotropic Electron-Photon and Electron-Phonon Interactions in Black Phosphorus

Xi Ling^{1¶}, Shengxi Huang^{1¶}, Eddwi H. Hasdeo², Liangbo Liang^{3,4}, William M. Parkin⁵, Yuki Tatsumi², Ahmad R. T. Nugraha², Alexander A. Puretzky⁴, Paul Masih Das⁵, Bobby G. Sumpter^{4,6}, David B. Geohegan⁴, Jing Kong¹, Riichiro Saito², Marija Drndic⁵, Vincent Meunier³, Mildred S. Dresselhaus^{1*}*

¹ Department of Electrical Engineering and Computer Science, Massachusetts Institute of Technology, Cambridge, Massachusetts 02139, USA.

² Department of Physics, Tohoku University, Sendai, 980-8578, Japan.

³ Department of Physics, Applied Physics, and Astronomy, Rensselaer Polytechnic Institute, Troy, New York 12180, USA.

⁴ Center for Nanophase Materials Sciences, Oak Ridge National Laboratory, Oak Ridge, Tennessee 37831, USA.

⁵ Department of Physics and Astronomy, University of Pennsylvania, Philadelphia, Pennsylvania 19104, USA.

⁶ Computer Science and Mathematics Division, Oak Ridge National Laboratory, Oak Ridge, Tennessee 37831, USA

[¶]These authors contributed equally to this work.

*** Corresponding Authors:**

Prof. Mildred S. Dresselhaus

**Department of Electrical Engineering and Computer Science,
Massachusetts Institute of Technology, Cambridge, Massachusetts 02139, USA**

Tel: +1-617-253-6864

Email: millie@mgm.mit.edu

Dr. Xi Ling

**Department of Electrical Engineering and Computer Science,
Massachusetts Institute of Technology, Cambridge, Massachusetts 02139, USA**

Tel: +1-617-253-6860

Email: xiling@mit.edu

This PDF file includes:

- S1. Polarized Raman scattering intensities of the flakes in Figure 1 under 532 nm laser excitation**
- S2. Polar plots of the Raman intensities versus the sample rotation angle for 13 BP flakes**
- S3. Energy band structures and band symmetry of BP with different thicknesses**
- S4. Analysis of the anisotropic absorption and Raman scattering using the selection rules of the optical transition**
- S5. Thickness dependence of absorbance of BP**
- S6. Polarized absorbance at 2.33 and 1.58 eV of BP flakes in Figure 2**
- S7. Polarized Raman scattering intensities of A_g^2 mode for the two typical flakes in Figure 2**
- S8. Semi-classical model of polarized Raman scattering**
- S9. Calculated anisotropic reflection and absorption of monolayer and bulk BP**
- S10. Calculated zigzag/armchair ratio of interference enhancement factor as a function of the sample thickness**

S1. Polarized Raman scattering intensities of the flakes in Figure 1 under 532 nm laser excitation

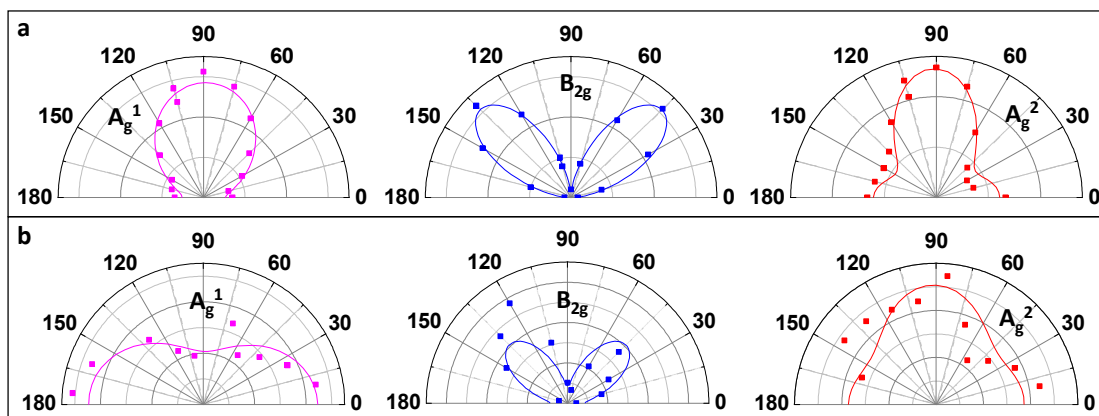


Figure S1. **a** and **b** are the Raman polarization dependence of the corresponding flakes in Figure 1c and d, respectively. **a** and **b** are both excited by 532 nm laser.

S2. Polar plots of the Raman intensities versus the sample rotation angle for 13 BP flakes

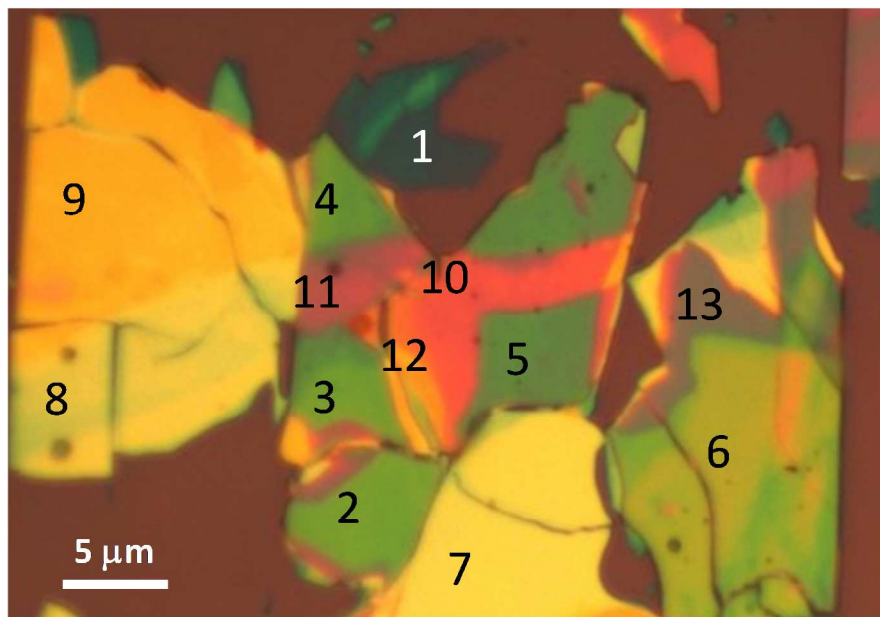
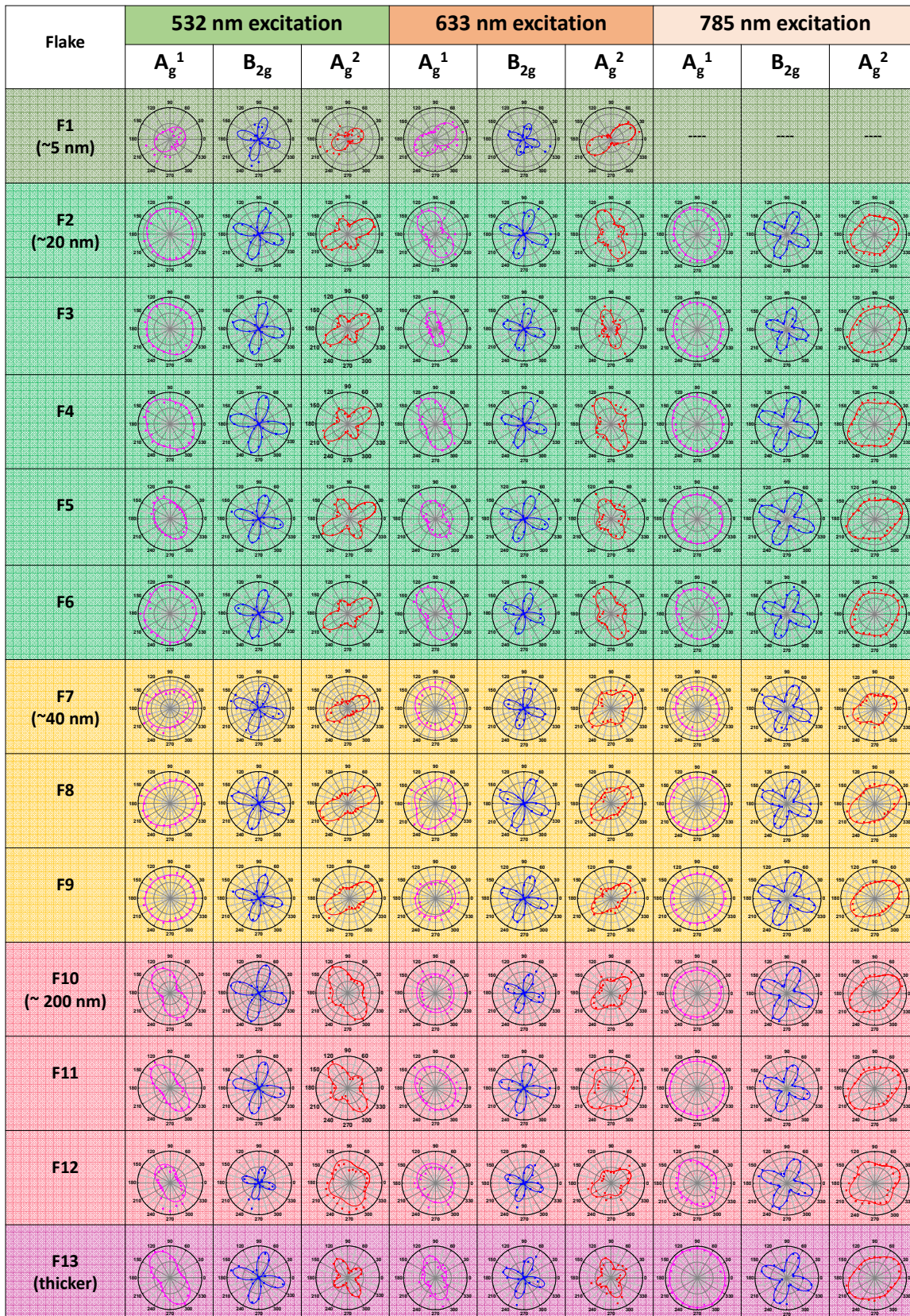


Figure S2. Optical image and assigned numbers of the BP flakes with different thicknesses. All of the flakes are physically connected to one another. The numbers from 1-13 are ordered by the thickness from thin to thick.

The optical image, as well as the numbering for the 13 flakes is shown in Figure S2. The crystalline orientations of these flakes are the same as the flakes in Table 1 of the main text, because they are physically connected to one another. The flakes are ordered according to their thicknesses. Similar thicknesses are shaded with the same color. Flakes 1, 2, 7, 10 correspond to flakes a, b, c, and d in the main text, respectively. Table S1 shows the corresponding polar plots of the profiles of the polarization dependence of A_g^1 , B_{2g} , and A_g^2 Raman modes from 13 different BP flakes, with excitation wavelengths 532 nm ($E_L=2.33$ eV), 633 nm ($E_L=1.96$ eV) and 785 nm ($E_L=1.58$ eV). It can be observed that flakes with similar thicknesses share the same orientation of main axis for Raman profiles for each mode under each laser excitation wavelength. The table indicates that the polarization profile is strongly dependent on the flake thickness. For each thickness, different laser wavelength renders different main axes for Raman profiles, which corroborates the conclusion drawn in the main text that the Raman profile is related to laser wavelength.

Table S1. Polar plots of the Raman intensities versus the sample rotation angle for 13 different BP flakes. The excitation wavelengths are 532 nm ($E_L=2.33$ eV), 633 nm ($E_L=1.96$ eV) and 785 nm ($E_L=1.58$ eV). The crystalline orientations of these flakes are the same as the flakes in Table 1 of the main text, because the flakes are physically connected to one another. The flake numbers are the order of thicknesses, and are labeled in the optical image in Figure S2. Similar thicknesses are shaded with the same color. Flakes 1, 2, 7, 10 correspond to flakes a, b, c, and d in Table 1 in the main text, respectively.



S3. Energy band structures and band symmetry of BP with different thicknesses

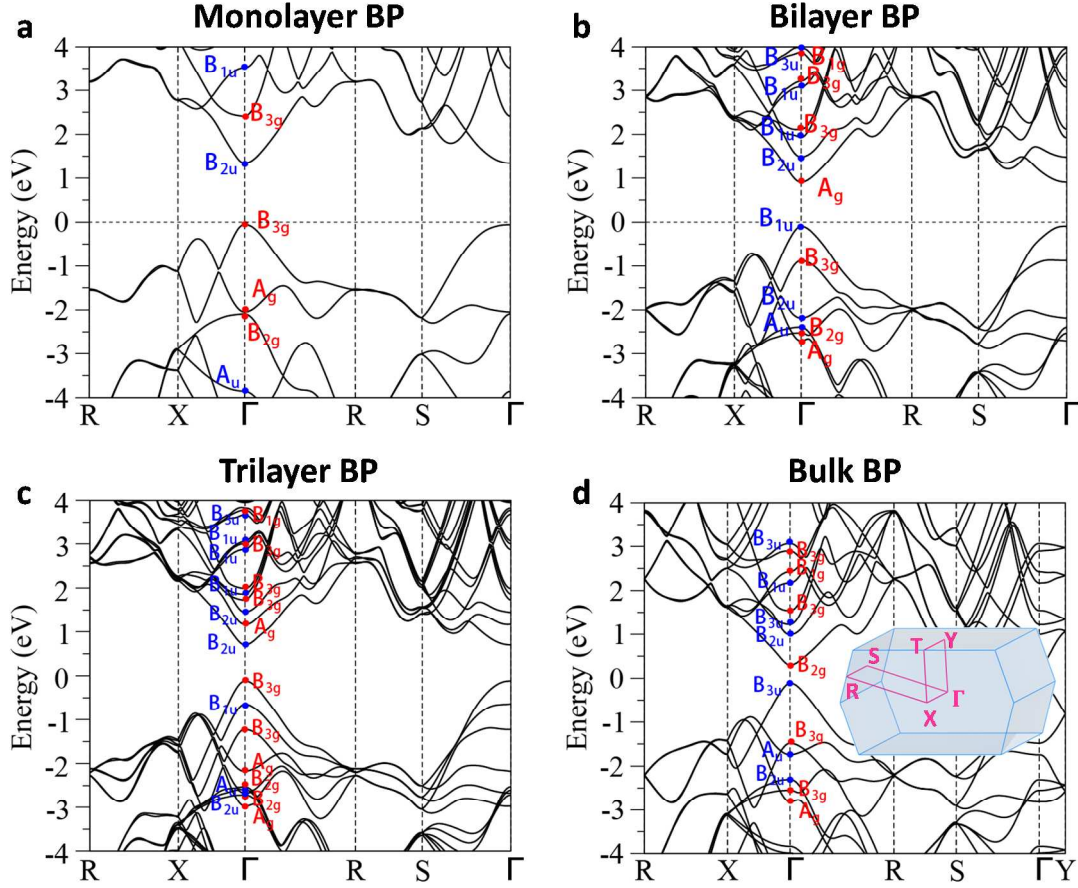


Figure S3. Band structures and band symmetry of BP with different thicknesses. a, monolayer BP; **b,** bilayer BP; **c,** trilayer BP; **d,** bulk BP. Red (blue) labels of irreducible representation correspond to symmetric (anti-symmetric) states under inversion symmetry. Inset of **d**: Brillouin zone of bulk BP with high symmetry points labeled. The coordinates of high symmetry points in the Brillouin zone in **a-c** are labeled in the inset of Figure 3a in the main text.

S4. Analysis of anisotropic absorption and Raman scattering using the selection rules of the optical transition

As mentioned in the main text, we first employed the generalized gradient approximation (GGA) using the PBE functional in the DFT calculation. Since conventional DFT tends to underestimate

energy separations between valence and conduction bands, electronic bands were then updated by the hybrid functional (HSE06) method, which has proven to yield a better description of electronic properties.^{1,2,3} From group theory analysis, the optical transition from the valence band maximum to the conduction band minimum at the Γ point is permitted but is only allowed for armchair-polarized light due to the selection rule.⁴ Similar to the case monolayer BP, we can expect armchair-polarized light absorption at around the energy gap for 2L, 3L and bulk BP.

BP of all thicknesses from monolayer to bulk belong to space group D_{2h} which has 3 rotation axes, 3 mirror planes and inversion symmetry.⁴ The symmetry properties of the BP family are distinguished by the translational symmetry indicated by the superscript of the space group label, i.e. D_{2h}^7 for odd number of layer BP, D_{2h}^{11} for even number of layer BP, and D_{2h}^{18} for bulk BP. Due to this similarity, it is useful to discuss the absorption and Raman selection rule based on the symmetry properties of 1L phosphorene.

According to the character table of D_{2h}^7 group (Table S2), we find the symmetry assignment for all bands of monolayer BP at the Γ point as shown in Figure S3a. For a given incoming light beam with polarization \mathbf{P} , there is an optical selection rule of the intermediate state m based on the dipole approximation matrix element given by:

$$\langle m | H_{\text{op}} | i \rangle = \frac{e\hbar}{m_e\omega} \sqrt{\frac{I_0}{c\epsilon_0}} \exp(-i\omega t) \mathbf{P} \cdot \mathbf{D}_{mi} \quad (\text{S1})$$

where e , m_e , c , ϵ_0 , and \mathbf{P} are, respectively, the unit electron charge, electron mass, speed of light, vacuum dielectric constant, and light polarization vector. The dipole vector \mathbf{D}_{mi} is defined by $\mathbf{D}_{mi} = \langle m | \nabla | i \rangle$, with the electronic wavefunctions $|i\rangle$ and $|m\rangle$ expressed by a linear

combination of plane waves.

As stated in the main text, in order to obtain non-vanishing electron-photon matrix elements for the optical transition from the state $|i\rangle$ to $|m\rangle$, we need to have

$$\Gamma_D \otimes \Gamma_i \subset \Gamma_m \quad (\text{S2})$$

where Γ_D , Γ_i , and Γ_m are the irreducible representations of D_{\parallel} (i.e. parallel component of \mathbf{D}_{mi} with respect to \mathbf{P}), $|i\rangle$, and $|m\rangle$, respectively. From Table S2, there are only two possible irreducible representations for Γ_D , namely, B_{1u} for the armchair-polarized light and B_{3u} for the zigzag-polarized light. Since Γ_i is given, we can thus construct a selection rule for the possible Γ_m at any given direction of \mathbf{P} , which are listed in Tables S3 and S4, for these cases, explicitly.

Table S2. Character table for the Γ point of monolayer BP. Monolayer BP belongs to the space group D_{2h}^7 at the Γ point.⁵ Here, SG and PG denote the space group and point group, respectively. The y - and z - axes have been swapped from Ref.5, according to the definition in Figure 1a, and are given here for consistency.

SG	PG	$\{E 0\}$	$\{C_{2x(z=1/4)} \tau_x^{(1)}\}$	$\{C_{2y(x=z=1/4)} 0\}$	$\{C_{2z} 0\}$	$\{i 0\}$	$\{\sigma_{xy} 0\}$	$\{\sigma_{xz} \tau_{xz}^{(2)}\}$	$\{\sigma_{yz(x=1/4)} \tau_z^{(3)}\}$	Basis
Γ_1^+	A_g	1	1	1	1	1	1	1	1	x^2, y^2, z^2
Γ_2^+	B_{1g}	1	1	-1	-1	1	-1	-1	1	yz
Γ_3^+	B_{2g}	1	-1	1	-1	1	-1	1	-1	xz
Γ_4^+	B_{3g}	1	-1	-1	1	1	1	-1	-1	xy
Γ_1^-	A_u	1	1	1	1	-1	-1	-1	-1	

Γ_2^-	B_{1u}	1	1	-1	-1	-1	1	1	-1	x
Γ_3^-	B_{2u}	1	-1	1	-1	-1	1	-1	1	y
Γ_4^-	B_{3u}	1	-1	-1	1	-1	-1	1	1	z

⁽¹⁾ $\boldsymbol{\tau}_x = \mathbf{a}_1/2$; ⁽²⁾ $\boldsymbol{\tau}_{xz} = (\mathbf{a}_1 + \mathbf{a}_3)/2$; ⁽³⁾ $\boldsymbol{\tau}_z = \mathbf{a}_3/2$, where $\mathbf{a}_1 = 4.29 \text{ \AA} \hat{x}$ and $\mathbf{a}_3 = 3.25 \text{ \AA} \hat{z}$, are lattice vectors along armchair and zigzag axes, respectively.

The Raman scattering process involves three steps: (1) electron excitation from an initial state i to an excited state m through photon absorption with polarization \mathbf{P}^i , (2) interaction of the excited electron with a phonon resulting in transition from the state m to m' , and finally (3) emission of a scattered photon with polarization \mathbf{P}^f and an electron transition from the state m' to the final state f , which is the same as the initial state i . Therefore, the E_L -dependent Raman intensity for the ν phonon mode (in arbitrary units) can be written as:

$$I_\nu(E_L) = \left| \sum_{i,m,m'} \frac{\langle f | H_{\text{OP}} | m' \rangle \langle m' | H_{\text{ep}}^\nu | m \rangle \langle m | H_{\text{OP}} | i \rangle}{(E_L - \Delta E_{mi})(E_L - \hbar\omega_\nu - \Delta E_{m'i})} \right|^2 \quad (\text{S3})$$

Where $\langle f | = \langle i |$, E_L is the excitation laser photon energy, $\Delta E_{mi} = E_m - E_i - i\gamma$, while E_i (E_m , $E_{m'}$) is the energy of the electronic state i (m , m'), and γ is the broadening factor. In our DFT calculation of polarized Raman intensity, we assume that H_{ep}^ν does not have a polarization dependence, but depending on incoming and outgoing polarization, H_{ep}^ν selects the intermediate states m and m' by symmetry selection rule. Therefore, the polarization dependence of the Raman intensity for different modes ν can be discussed by imposing the group theory selection rule for choosing the most relevant intermediate states m and m' . From equation (S3), the

condition for obtaining the intensity value is that $\Gamma_{\text{op}}^{\text{fm}'} \otimes \Gamma_{\text{ep}}^{\text{m}'\text{m}} \otimes \Gamma_{\text{op}}^{\text{mi}} \subset A_g$, where $\Gamma_{\text{op}}^{\text{fm}'}$, $\Gamma_{\text{ep}}^{\text{m}'\text{m}}$, $\Gamma_{\text{op}}^{\text{mi}}$ are the irreducible representations of the dipole vector component parallel to \mathbf{P}^f , the electron-phonon (e-p) interaction, and the dipole vector component parallel to \mathbf{P}^i , respectively (see again the description of these quantities in the main text).⁴ Hereafter, we use a shorthand notation xz -polarization for describing a Raman experiment with incoming armchair-polarized light and outgoing zigzag-polarized light. The remaining polarization conditions xx , zx , and zz are defined accordingly. Depending on the incoming and outgoing \mathbf{P} , we can excite two types of phonon symmetries, namely the A_g modes (A_g^1 and A_g^2) phonon modes for the xx - and zz -polarizations, and the B_{2g} phonon mode for either xz - or zx -polarization. If the incoming and outgoing polarizations are parallel (not parallel) to each other, the symmetry of $|m\rangle$ and $|m'\rangle$ should be equal (different). The selection rules for $|m\rangle$ and $|m'\rangle$ for a given initial state i and for the two given polarization directions are summarized in Tables S3 and S4.

Table S3. Selection rules for intermediate states m and m' for a given initial state $|i\rangle$ and for polarization vector xx or zz which both correspond to the A_g phonon excitation. These selection rules correspond to the following product of matrix elements:

$$\langle f|H_{\text{op}}|m'\rangle\langle m'|H_{\text{ep}}(A_g)|m\rangle\langle m|H_{\text{op}}|i\rangle \text{ with } \langle f| = \langle i|.$$

xx		zz	
$ i\rangle$	$ m\rangle = m'\rangle$	$ i\rangle$	$ m\rangle = m'\rangle$
A_g	B_{1u}	A_g	B_{3u}
B_{1g}	A_u	B_{1g}	B_{2u}
B_{2g}	B_{3u}	B_{2g}	B_{1u}
B_{3g}	B_{2u}	B_{3g}	A_u
A_u	B_{1g}	A_u	B_{3g}
B_{1u}	A_g	B_{1u}	B_{2g}
B_{2u}	B_{3g}	B_{2u}	B_{1g}
B_{3u}	B_{2g}	B_{3u}	A_g

Table S4. Selection rules for intermediate states m and m' for a given initial state $|i\rangle$ and polarization vector xz or zx which both correspond to the B_{2g} phonon excitation. These selection rules correspond to the following product of matrix elements:

$$\langle f|H_{\text{op}}|m'\rangle\langle m'|H_{\text{ep}}(B_{1g})|m\rangle\langle m|H_{\text{op}}|i\rangle, \text{ with } \langle f| = \langle i|.$$

xz			zx		
$ i\rangle$	$ m\rangle$	$ m'\rangle$	$ i\rangle$	$ m\rangle$	$ m'\rangle$
A_g	B_{1u}	B_{3u}	A_g	B_{3u}	B_{1u}
B_{1g}	A_u	B_{2u}	B_{1g}	B_{2u}	A_u
B_{2g}	B_{3u}	B_{1u}	B_{2g}	B_{1u}	B_{3u}
B_{3g}	B_{2u}	A_u	B_{3g}	A_u	B_{2u}
A_u	B_{1g}	B_{3g}	A_u	B_{3g}	B_{1g}
B_{1u}	A_g	B_{2g}	B_{1u}	B_{2g}	A_g
B_{2u}	B_{3g}	B_{1g}	B_{2u}	B_{1g}	B_{3g}
B_{3u}	B_{2g}	A_g	B_{3u}	A_g	B_{2g}

In Figure S4, we show the polarization dependence of the absorption intensity and Raman intensity of trilayer BP. We consider two optical transitions which are allowed by symmetry, such as the $B_{1u} \rightarrow A_g$ transition with $E_L = 2.00$ eV (Figure S4a,b) and $A_g \rightarrow B_{3u}$ transition with $E_L = 5.86$ eV (Figure S4a,c). The former (latter) gives the maximum absorption intensity along the armchair (zigzag) polarization and minimum absorption intensity along the zigzag (armchair) polarization direction.

Now, when we consider the Raman process, there will be phonon excitations represented by intermediate states $|m\rangle$ and $|m'\rangle$. Suppose that the initial state has the B_{1u} symmetry. If $|m\rangle = |m'\rangle$, from the selection rules we find the corresponding phonon mode that can be excited strongly is the A_g mode. For example, if the intermediate states are the A_g conduction band shown in Figure S3c and Figure S4a, the transition will be allowed for the B_{1u} initial state with armchair-polarization. Such a case is shown in Figure S4d, in which the shape of the polar plot is the square of the polar plot in Figure S4b. Similarly, for the allowed transition of the B_{2g} phonon mode, selection rules suggest that $|m\rangle$ and $|m'\rangle$ have different symmetries, and the shape of the polar plot is the product of the shapes in Figure S4b-c (not in scale), shown in Figure S4e. Such a concept should also be similar when applied to the other BP flakes with different number of layers, and also for the bulk BP. Therefore, depending on the laser energy and the band symmetry, we can have a variety of polarization dependences for the absorption and Raman spectra.

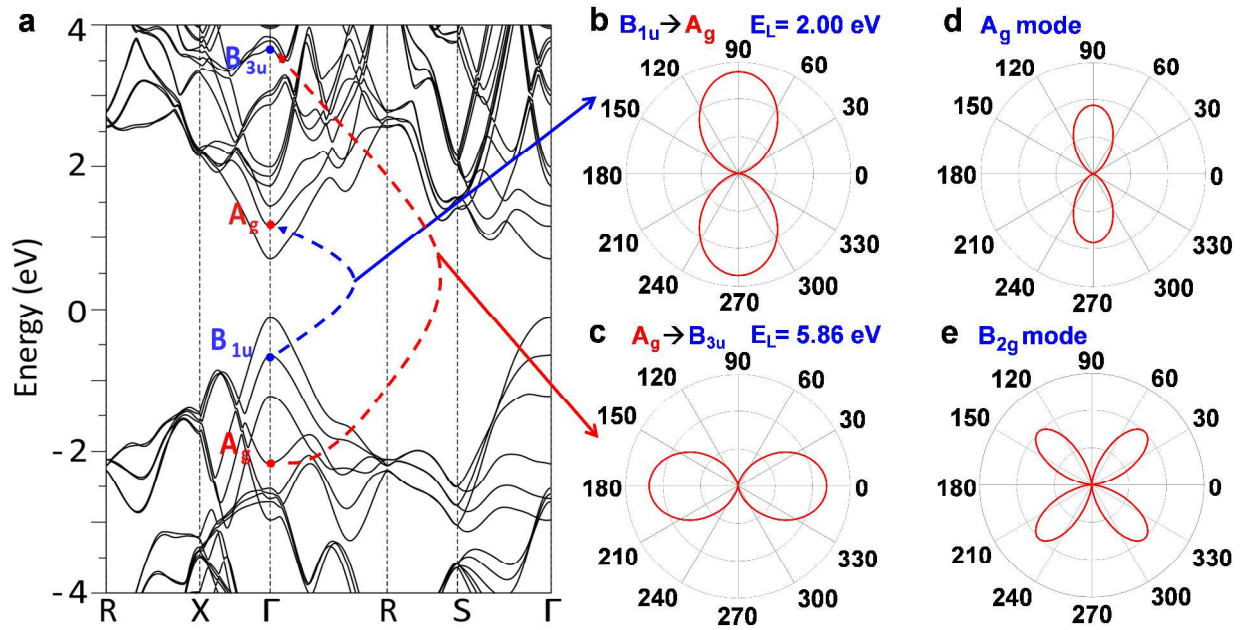


Figure S4. Calculated polarization dependence of the absorption intensity and the Raman intensity in trilayer BP for two optical transitions allowed by symmetry. **a**, Calculated electronic band structure $E(k)$ of trilayer BP. A_g bands are indicated by red labels while B_{1u} and B_{3u} bands are indicated by blue labels at the Γ point. **b,c**, Two different possible optical transitions in trilayer BP with the corresponding symmetry assignments. The absorption intensity is defined by the square of optical matrix elements. **d,e**, Schematic diagram for the Raman intensity of the A_g mode (**d**) and the B_{2g} mode (**e**).

S5. Thickness dependence of the absorbance of BP

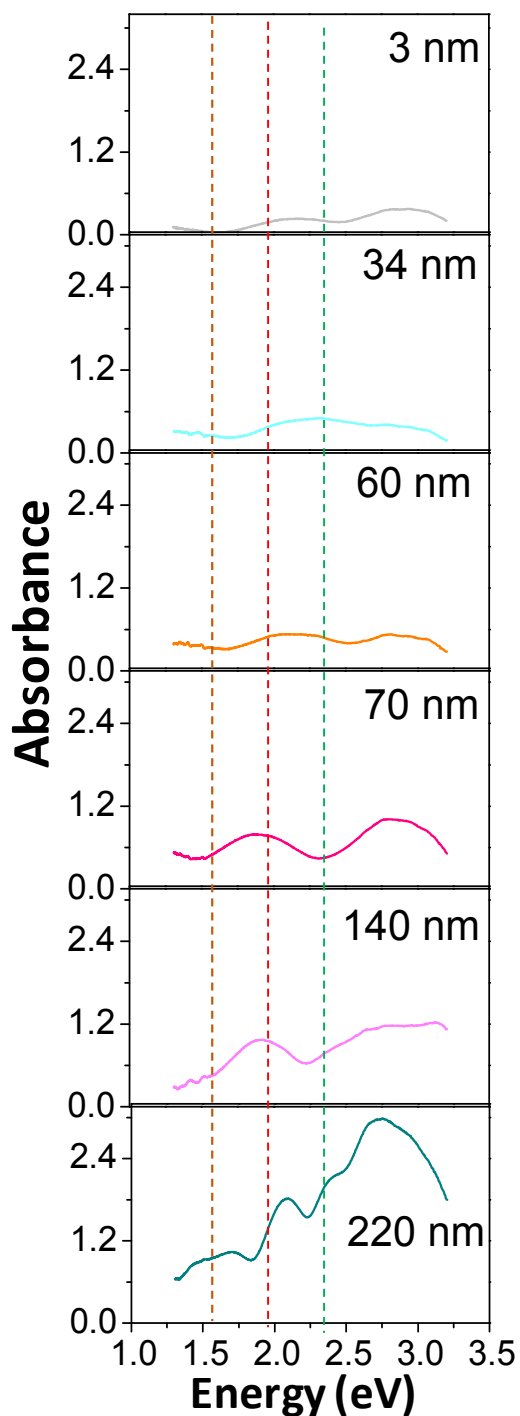


Figure S5. Thickness dependence of the optical absorbance on BP. Absorbance spectra for BP flakes for various thicknesses from 3 nm to 220 nm. The three vertical dashed lines indicate the positions of optical wavelengths 532 nm (2.33 eV) (green), 633 nm (1.96 eV) (red) and 785 nm (1.58 eV) (orange). The incident light is unpolarized.

S6. Polarized absorbance at 2.33 and 1.58 eV of BP flakes in Figure 2

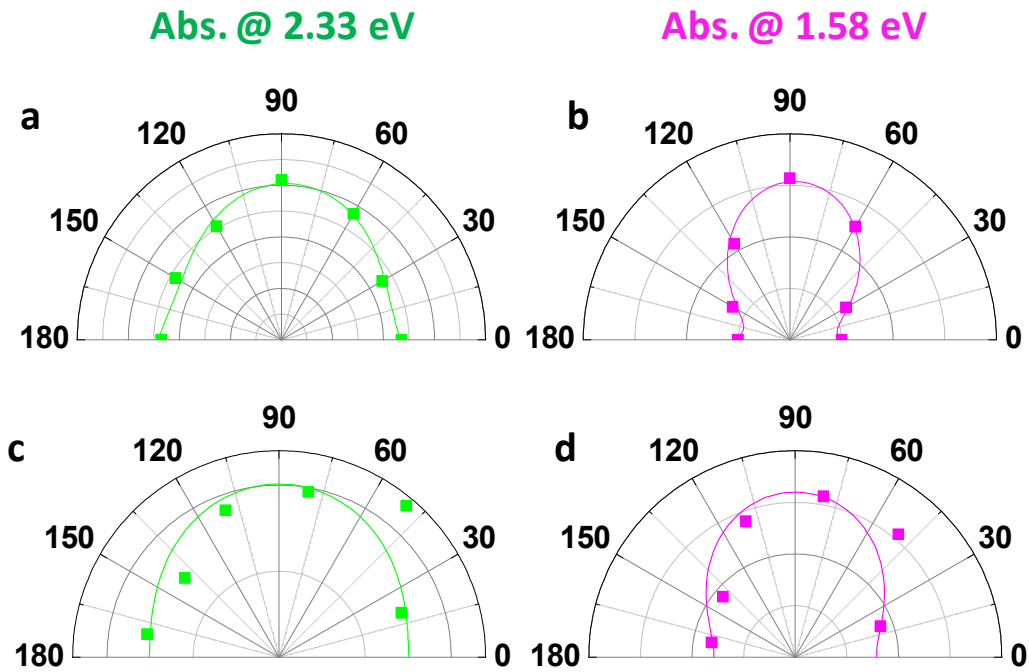


Figure S6. Polar plots of the absorbance at 2.33 eV (in green) and 1.58 eV (in pink) of BP versus the sample rotation angle. a,b, corresponding to the thin flake (9 nm) in Figure 2b; c,d, corresponding to the thick flake (225 nm) in Figure 2c. The points are experimental data and the colored solid curves are numerical fittings.

S7. Polarized Raman scattering intensities of A_g^2 mode for the two typical flakes in Figure 2

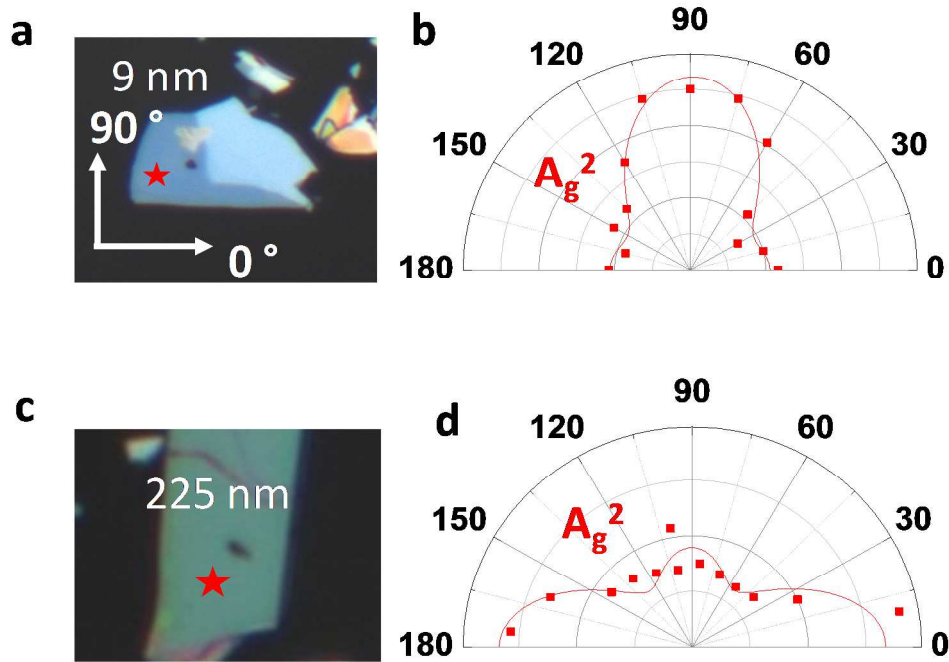


Figure S7. Optical images and the corresponding polar plots of the A_g^2 Raman intensities versus the sample rotation angle. a,b, corresponding to the thin BP flake in Figure 2b; c,d, corresponding to the thick BP flake in Figure 2c.

S8. Semi-classical model of polarized Raman scattering

The anisotropic resonant Raman scattering can also be understood from a semi-classical perspective. Since the optical absorption coefficient at wavelength λ is $\alpha = 4\pi k/\lambda$, where k is the imaginary part of the refractive index, at a certain wavelength, the change of the absorbance spectrum with the crystalline orientation indicates that the refractive index ($n + ik$) depends on the crystalline orientation. Here n and k are subject to the constraints relating the frequency dependence of n and k according to the Kramers–Kronig relations.⁶ In addition, as there is a

relation between the refractive index and the dielectric function $((n + ik)^2 = \varepsilon_r + i\varepsilon_i)$, the anisotropic absorption indicates an anisotropic dielectric function, which needs careful evaluation for the case of BP and related anisotropic materials. Therefore, the Raman tensor elements, which are sensitive to both the real and imaginary parts of the dielectric function (ε_r and ε_i), as well as to the normal coordinates of the Raman mode, will change with crystalline orientation.

From group theory, we know that the Raman tensors for the A_g and B_{2g} modes are:^{7,8}

$$\tilde{R}_{A_g} = \begin{pmatrix} a & 0 & 0 \\ 0 & b & 0 \\ 0 & 0 & c \end{pmatrix}$$

$$\tilde{R}_{B_{2g}} = \begin{pmatrix} 0 & 0 & f \\ 0 & 0 & 0 \\ f & 0 & 0 \end{pmatrix}$$

in which

$$a = |a|e^{i\phi_a} = \frac{\partial \varepsilon_{xx}}{\partial q^{A_g}} = \frac{\partial \varepsilon'_{xx}}{\partial q^{A_g}} + i \frac{\partial \varepsilon''_{xx}}{\partial q^{A_g}}$$

$$b = |b|e^{i\phi_b} = \frac{\partial \varepsilon_{yy}}{\partial q^{A_g}} = \frac{\partial \varepsilon'_{yy}}{\partial q^{A_g}} + i \frac{\partial \varepsilon''_{yy}}{\partial q^{A_g}}$$

$$c = |c|e^{i\phi_c} = \frac{\partial \varepsilon_{zz}}{\partial q^{A_g}} = \frac{\partial \varepsilon'_{zz}}{\partial q^{A_g}} + i \frac{\partial \varepsilon''_{zz}}{\partial q^{A_g}}$$

$$f = |f|e^{i\phi_f} = \frac{\partial \varepsilon_{xz}}{\partial q^{B_{2g}}} = \frac{\partial \varepsilon'_{xz}}{\partial q^{B_{2g}}} + i \frac{\partial \varepsilon''_{xz}}{\partial q^{B_{2g}}}$$

where ε'_{ii} and ε''_{ii} ($i=x, y, z$) are the real and imaginary parts of the dielectric function along different crystalline orientations, and q^{A_g} and $q^{B_{2g}}$ are the normal coordinates of the Raman modes. The complex values of the Raman tensor elements are due to the light absorption of BP.

The intensity of the Raman modes can be calculated using:

$$I = |\hat{e}_i^T \tilde{R} \hat{e}_s|^2 \propto \left| (\sin \theta, 0, \cos \theta) \tilde{R} \begin{pmatrix} \sin \gamma \\ 0 \\ \cos \gamma \end{pmatrix} \right|^2$$

in which \hat{e}_i and \hat{e}_s are the light polarization vectors of the incident and scattered beams, respectively, θ is the angle between the incident laser polarization and the zigzag direction, and γ is the angle between the scattered light polarization and the zigzag direction.

Therefore, for parallel backscattering configuration, $\theta = \gamma$, so

$$I_{Ag}^{\parallel} = |a|^2 \left[(\sin^2 \theta + \left| \frac{c}{a} \right| \cos \Phi_{ca} \cos^2 \theta)^2 + \left| \frac{c}{a} \right|^2 \sin^2 \Phi_{ca} \cos^4 \theta \right] \quad (S4)$$

Here, Φ_{ca} is the phase difference between the complex Raman tensor elements c and a . From equation (S4), we see that whether $|c/a| > 1$ or $|c/a| < 1$ determines whether the main axis is along the zigzag direction or the armchair direction. Therefore, $|c/a|$ and Φ_{ca} , which have already been discussed in the literature,⁷ suggests that the thickness of the BP flake and the excitation photon wavelength, which are the measurable parameters, are most sensitive to the anisotropic properties of BP. From equation (S4), we know the polarized Raman intensity profile (the relation between I_{Ag}^{\parallel} and θ) which is a function of both $|c/a|$ and Φ_{ca} . Figure S8 plots the profiles for different $|c/a|$ and Φ_{ca} values. Some properties of the polarized Raman intensity are summarized below:

(1) Φ_{ca} is symmetric with respect to 180° : $I_{Ag}^{\parallel}(\Phi_{ca}) = I_{Ag}^{\parallel}(360^\circ - \Phi_{ca})$

(2) When $\theta = 0^\circ$ (zigzag), $I_{Ag,\theta=0^\circ}^{\parallel} = |c|^2$; when $\theta = 90^\circ$ (armchair), $I_{Ag,\theta=90^\circ}^{\parallel} = |a|^2$.

Therefore, $\frac{I_{Ag,\theta=0^\circ}^{\parallel}}{I_{Ag,\theta=90^\circ}^{\parallel}} = \left| \frac{c}{a} \right|^2$. This can be confirmed by the intensity values shown in Figure S8 for

different $|c/a|$. The same $|c/a|$ renders the same $\frac{I_{Ag,\theta=0^\circ}^{\parallel}}{I_{Ag,\theta=90^\circ}^{\parallel}}$, despite the different Φ_{ca} values.

(3) For the Raman intensity profile $I_{A_g}^{\parallel}(\theta)$, in the first quadrant ($\theta \in [0^\circ, 90^\circ]$, and in the other quadrants the Raman intensity profiles are repetitions or symmetric to the first quadrant), two maximum points occur when $\theta = 0^\circ$ and 90° . Except for these maximum points, there may be another minimum point, shown in the inset of Figure S8b. This minimum point occurs when

$$\tan^2 \theta_{min} = \frac{\left|\frac{c}{a}\right|^2 - \left|\frac{c}{a}\right| \cos \Phi_{ca}}{1 - \left|\frac{c}{a}\right| \cos \Phi_{ca}} \quad (S5)$$

and this gives $\frac{I_{A_g, min}^{\parallel}}{I_{A_g, \theta=0^\circ}^{\parallel}} = \frac{\sin^2 \Phi_{ca}}{1 + \left|\frac{c}{a}\right|^2 - 2\left|\frac{c}{a}\right| \cos \Phi_{ca}}$. These calculation results can be confirmed by the

values shown in Figure S8.

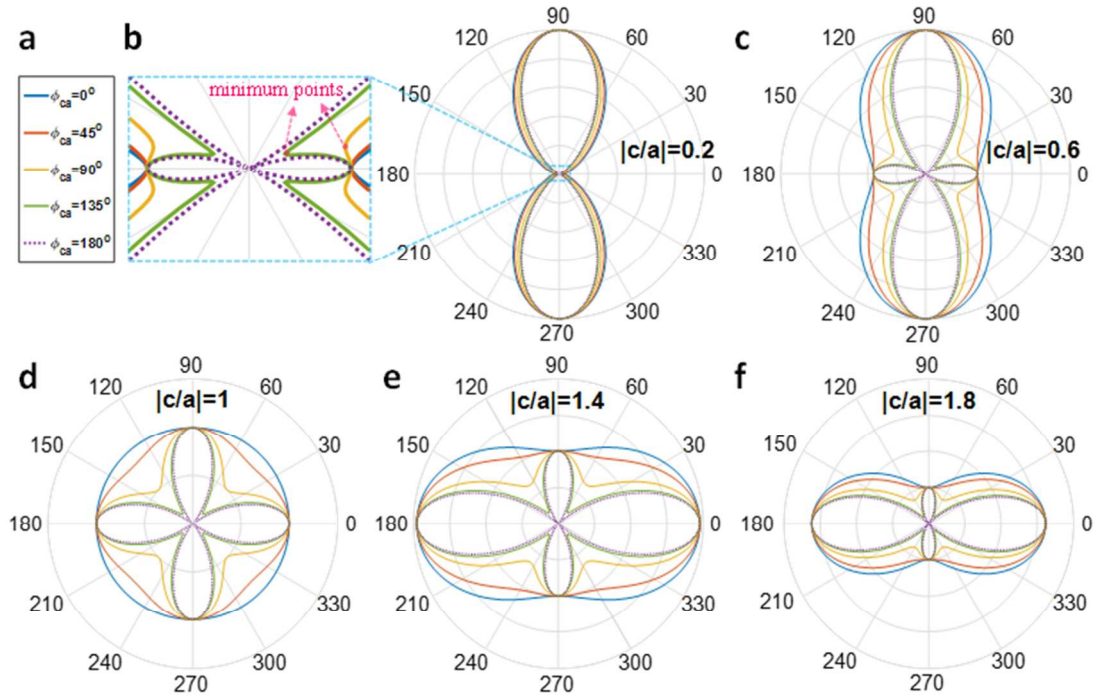


Figure S8. Polarized Raman intensity profiles of A_g modes with different $|c/a|$ and Φ_{ca} values. **a**, Legends showing the profile for different Φ_{ca} values from 0° to 180° . **b-f**, the profiles with different $|c/a|$ values, and each with the corresponding different Φ_{ca} values. The inset of **b** is a zoom-in profile when $|c/a| = 0.2$. The minimum points are indicated. All the intensities are normalized by the intensity values at $\theta=90^\circ$. 0° (90°) corresponding to the zigzag (armchair) direction.

S9. Calculated anisotropic reflection and absorption of monolayer and bulk BP

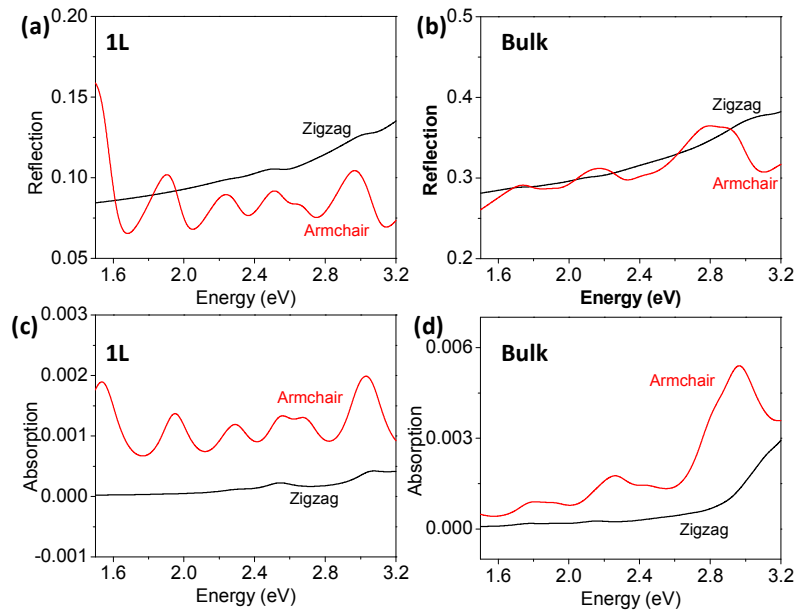


Figure S9. Calculated reflection (a-b) and absorption (c-d) spectra of monolayer (left) and Bulk (right) BP. Reflection and absorption with the light polarization along armchair (zigzag) direction is in red (black).

S10. Calculated zigzag/armchair ratio of interference enhancement factor as a function of the sample thickness

As shown in Figure S10 (a), for the three laser lines we used, the interference enhancement is stronger when the incident polarization is along the zigzag direction, consistent with Ref. 17 in the maintext. The ratio of the enhancement factors between the zigzag and the armchair directions varies significantly with the BP thickness, which in turn can influence the thickness dependence of Raman intensity ratio $|c/a|$ between the zigzag and the armchair directions. In Figures 4(c-d), we eliminate the effect of interference on Raman intensity, and thus the $|c/a|$ and Φ_{ca} values shown are intrinsically from the BP flakes. While $|c/a|$ ratios do not show

a clear evolution trend in Figure 4(a), the $|c/a|$ ratios in Figure 4(c) show a roughly increasing trend with increasing thicknesses and are generally smaller than 1, in agreement with Ref. 17 in the maintext. This suggests that after elimination of interference effect, the maximum intensities of anisotropic Raman are generally along the armchair direction, thus the thickness dependence becoming simpler.

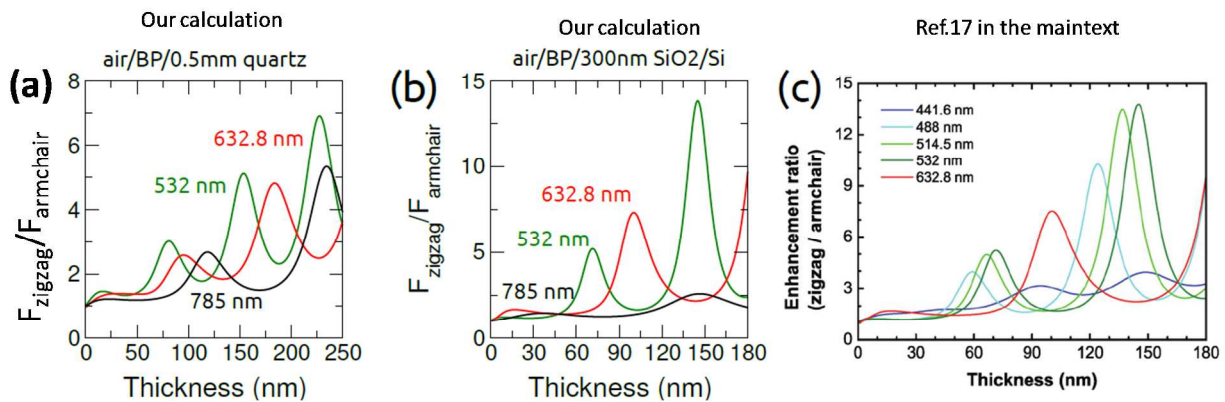


Figure S10. Calculated zigzag/armchair ratio of interference enhancement factor as a function of the sample thickness for different excitation wavelengths for (a) air/BP/0.5-mm-quartz and (b,c) air/BP/300-nm-SiO₂/Si configurations. (a, b) are our calculation results; (c) is the results of Ref. 17 in the maintext.

References

- (1) Tran, V.; Soklaski, R.; Liang, Y.; Yang, L. *Phys. Rev. B* **2014**, *89* (23), 235319.
- (2) Qiao, J.; Kong, X.; Hu, Z.-X.; Yang, F.; Ji, W. *Nat. Commun.* **2014**, *5*.
- (3) Dai, J.; Zeng, X. C. *J. Phys. Chem. Lett.* **2014**, *5* (7), 1289–1293.
- (4) Takao, Y.; Morita, A. *Phys. BC* **1981**, *105* (1-3), 93–98.
- (5) Ribeiro-Soares, J.; Almeida, R. M.; Cançado, L. G.; Dresselhaus, M. S.; Jorio, A. *Phys. Rev. B* **2015**, *91* (20), 205421.
- (6) Fox, M. *Optical properties of solids*, 2nd ed.; Oxford master series in condensed matter physics; Oxford University Press: Oxford ; New York, 2010.
- (7) Ribeiro, H. B.; Pimenta, M. A.; de Matos, C. J. S.; Moreira, R. L.; Rodin, A. S.; Zapata, J. D.; de Souza, E. A. T.; Castro Neto, A. H. *ACS Nano* **2015**, *9* (4), 4270–4276.

- (8) Ling, X.; Liang, L.; Huang, S.; Poretzky, A. A.; Geohegan, D. B.; Sumpter, B. G.; Kong, J.; Meunier, V.; Dresselhaus, M. S. *Nano Lett.* **2015**, *15* (6), 4080–4088.